INTERNATIONAL JOURNAL OF CLIMATOLOGY
Int. J. Climatol. (2010)
Published online in Wiley Online Library
(wileyonlinelibrary.com) DOI: 10.1002/joc.2217

Different impacts of El Niño and El Niño Modoki on China rainfall in the decaying phases

Juan Feng,[a] Wen Chen,[a,b]* C.-Y. Tam[c,d] and Wen Zhou[c,d]

[a] *Center for Monsoon System Research, Institute of Atmospheric Physics, Chinese Academy of Sciences, Beijing, China*
[b] *LASG, Institute of Atmospheric Physics, Chinese Academy of Sciences, Beijing, China*
[c] *CityU-IAP Laboratory for Atmospheric Sciences, City University of Hong Kong, Hong Kong, China*
[d] *Guy Carpenter Asia-Pacific Climate Impact Centre, School of Energy and Environment, City University of Hong Kong, Hong Kong, China*

ABSTRACT: In this study, we investigate the different impacts of El Niño and El Niño Modoki on China rainfall in their decaying phases. During spring, in the decaying year of El Niño events, there are positive rainfall anomalies south of the Yangtze River, whereas no obvious rainfall signals are found in the same season for the decaying El Niño Modoki. In the subsequent summer season, the wet signal south of the Yangtze River associated with El Niño continues, while suppressed rainfall now appears in the northern Yangtze–Huaihe River region. In contrast, the rainfall is above normal in the region from the Huaihe River to the Yellow River, and below normal in southern China during the summer of the decaying El Niño Modoki events. The distinct China rainfall anomaly is mainly attributed to the difference between the evolution and location of the anomalous western North Pacific (WNP) anti-cyclone associated with El Niño and El Niño Modoki events. For the case of El Niño, the WNP anti-cyclone brings plentiful moisture to southern China; meanwhile it shifts the ridge of sub-tropical high westward in both spring and summer. These tend to induce positive rainfall anomalies in the southern Chinese region. In contrast, due to fast decaying of El Niño Modoki, the anomalous WNP anti-cyclone becomes weak so that there are no significant rainfall anomalies in China. In summer, however, the WNP anti-cyclone re-invigorates possibly associated with a subsequent developing La Niña and extends more northwestward towards the inland region, compared to its El Niño counterpart. The anomalous moisture transport and sub-tropical high activity associated with this WNP anti-cyclone result in different summer rainfall anomalies in China. Copyright © 2010 Royal Meteorological Society

KEY WORDS El Niño; El Niño Modoki; China rainfall; anomalous WNP anti-cyclone

Received 2 February 2010; Revised 7 July 2010; Accepted 29 July 2010

1. Introduction

The El Niño-Southern oscillation (ENSO) is a coupled ocean-atmosphere phenomenon in the tropical Pacific, which has an important influence on the East Asian summer monsoon (EASM) (e.g. Weng *et al*., 1999; Zhang *et al*., 1999; Chang *et al*., 2000; Huang *et al*., 2004; Chan and Zhou, 2005; Zhou and Chan, 2007; Zhou *et al*., 2009). The relationship between the ENSO and EASM is complicated, and researchers have employed different methods to reveal its different facets. Lin and Yu (1993) classified the El Niño events into the eastern Pacific pattern and the central Pacific pattern according to the location of the onset of warm sea surface temperature (SST) anomalies. They analysed the summer precipitation anomaly after the mature phase of El Niño and found that eastern Pacific pattern El Niño causes deficient rainfall over the Yangtze River Valley, while excessive rainfall is found in North China and the south of Yangtze River. On the other hand, central Pacific pattern El Niño induces the opposite anomalous rainfall pattern. A schematic map of China with three major rivers marked is shown in Figure 1(a). Xue and Liu (2008) defined two types of El Niño based on its intensity, namely moderate El Niño and strong El Niño, and found that they have different impacts on China rainfall. Several studies also documented El Niño-related rainfall variations in China in different stages of ENSO. Huang and Wu (1989) reported that in the developing stage of El Niño, drought is present in southern and northern China, while flood occurs over the Yangtze–Huaihe River Valley. The rainfall anomalies are reversed in the summer after the peak of El Niño. Similar results were also obtained by Chen (2002) and Liu and Ding (1992). Wu *et al*. (2003) further investigated the influence of the different phases of El Niño on the East Asian rainfall anomaly and proposed two El Niño-related rainfall anomaly centres. The positive one, induced by the anomalous low-level anti-cyclone over western North Pacific (WNP), covers southern China, eastern central China and southern Japan from the fall of an El Niño developing year till the following spring. The negative centre of action is over northern China during the summer and fall of an El Niño developing year, which is influenced by the anomalous barotropic cyclone over East Asia. Particularly, the anomalous WNP anti-cyclone

* Correspondence to: Wen Chen, Institute of Atmospheric Physics, Chinese Academy of Sciences, P. O. Box 2718, Beijing 100190, China.
E-mail: cw@post.iap.ac.cn

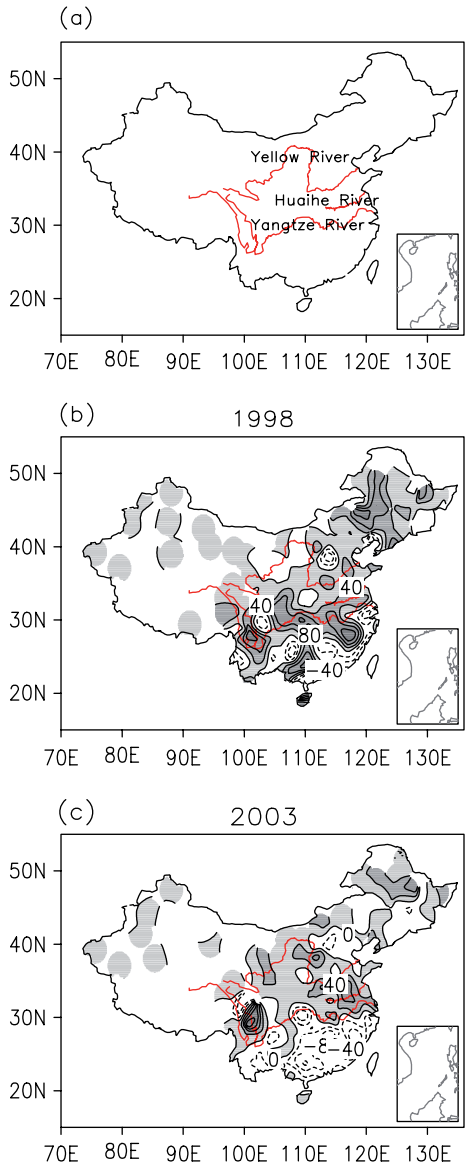

Figure 1. (a) The schematic map of China with the Yellow, Huaihe and Yangtze Rivers marked. (b) The summer rainfall anomalies in 1998. (c) The summer rainfall anomalies in 2003. The contour interval is 40 mm/month and the shading denotes the positive values in (b) and (c). This figure is available in colour online at wileyonlinelibrary.com/journal/joc

has been documented to be directly related to the rainfall anomalies in China (Zhang *et al*., 1996). This key system is also pointed out by Wang *et al*. (2000), who found that the anomalous anti-cyclone is confined to the lower troposphere and can bring more moisture to East Asia.

Recently, a new type of El Niño has been proposed (Ashok *et al*., 2007), which is characterized by a warm tropical sea surface temperature anomaly (SSTA) in the central equatorial Pacific and cold SSTA in the western and eastern Pacific. This is called 'El Niño Modoki', in order to distinguish it from the canonical El Niño. El Niño Modoki is defined by the second SSTA mode from empirical orthogonal function (EOF) analysis, which can explain about 12% of its variance (Ashok *et al*., 2007). It is found that El Niño Modoki significantly influences the climate over many parts of the globe. More importantly, the induced climate anomaly is very different from that associated with the conventional El Niño (e.g. Ashok *et al*., 2007, 2009b; Weng *et al*., 2007; Huang and Huang, 2009; Taschetto *et al*., 2009). Taschetto *et al*. (2009) found that Modoki and non-Modoki El Niño exhibit marked different impacts on the Australian rainfall. El Niño Modoki was also shown to influence the climate of the Pacific Rim countries including China, Japan and America (Weng *et al*., 2007).

Finally, it is well known that ENSO is an important predictor of EASM. During the typical El Niño of 1997–1998 (McPhaden, 1999; Picaut *et al*., 2002), the Yangtze River Valley suffered a severe flood in 1998 summer (Figure 1(b)). The National Climate Center (NCC) of the Chinese Meteorological Administration succeeded in predicting the flooding event. However, NCC failed to forecast the excessive rainfall over the Huaihe River in 2003 (Figure 1(c)). This is because seasonal forecasts were made according to the classic El Niño rainfall pattern, which is characterized by enhanced precipitation in the Yangtze River Valley and suppressed one in the Huaihe River Valley. However, SSTAs in 2002–2003 were not typical of a canonical El Niño event. In fact, positive SSTA is confined to the central Pacific (McPhaden, 2004; Bao and Han, 2009), indicative of an El Niño Modoki condition. This highlights the practical importance of distinguishing between the two types of El Niño and their climatic impacts.

The objective of this work is to explore the different impacts of El Niño and El Niño Modoki on the rainfall over China. Since the impact of El Niño on rainfall is more significant in its decaying than in its developing stage, attention is paid to the years of decaying El Niño and El Niño Modoki. The discussion of the text is as follows: Section 2 describes the data and methods used in this study. Section 3 shows the evolution of the SSTA in El Niño and El Niño Modoki, followed by comparisons of anomalous rainfall patterns in China during the decaying stage of the two types of El Niño. Possible mechanisms responsible for the different rainfall anomalies are discussed in Section 4. Conclusions are given in Section 5.

2. Data and methods

The Hadley Centre global sea ice and sea surface temperature (HadISST) analysis datasets (Rayner *et al*., 2003) are used in this study. It is a unique combination of monthly globally complete fields of SST and sea ice concentration on a 1° latitude–longitude grid. The monthly station rainfall data including 160 stations are provided by Chinese Meteorological Data Center, covering the years from 1951 to 2008. The atmospheric data are obtained from the National Centers for Environmental Prediction–National Center for Atmospheric Research (NCEP–NCAR) reanalysis (Kalnay *et al*., 1996). The horizontal resolution of these datasets is 2.5° × 2.5°. The

data period used in this article is from 1955 to 2005. Since the Indo-western Pacific climate response to ENSO experienced an inter-decadal change across the mid-1970s (Xie *et al*., 2010), we exclude this inter-decadal variation by removing the variability with periods over 7 years through the Lanczos filtering method (Duchon, 1979) before the data are used.

Conventional El Niño events are identified by the normalized 3-month running mean Niño3 SSTAs exceeding 0.5 and persisting for 8 months (Figure 2). According to this definition, eight major El Niño events (1957/1958, 1965/1966, 1969/1970, 1972/1973, 1976/1977, 1982/1983, 1987/1988 and 1997/1998) are identified. For El Niño Modoki events, we use the El Niño Modoki index (EMI) defined by Ashok *et al*. (2007):

$$\mathrm{EMI} = [\mathrm{SSTA}]_{\mathrm{A}} - 0.5[\mathrm{SSTA}]_{\mathrm{B}} - 0.5[\mathrm{SSTA}]_{\mathrm{C}} \qquad (1)$$

The brackets in Equation (1) represent the area-averaged SSTA over the region A (165 °E–140 °W, 10 °S–10°N), B (110 °W–70 °W, 15 °S–5°N) and C (125 °E–145 °E, 10 °S–20°N). The El Niño Modoki events are identified by requiring the normalized 3-month running mean EMI to be no less than 0.7 and persist for 7 months. In addition, we also require that the maximum SSTA in the central Pacific exceeds 1.0 °C in the peak phase of an event. On the basis of these criteria, we identified five major El Niño Modoki events (1963/1964, 1977/1978, 1994/1995, 2002/2003 and 2004/2005; Figure 2(b)). Note that the years 1965/1966, 1966/1967 and 1967/1968 are not selected because the second criterion is not satisfied. They are all characterized by a strong negative SSTA in the eastern Pacific and a very weak positive SSTA in the central Pacific. In addition, the EMI in 1963/1964 meets the criteria of El Niño Modoki, while the Nino3 index greater than 0.5 can also persist for 6 months from June to November. However, when looking at the evolution of the SSTA from 1963 to 1964, we found that the warming is largely confined to the central Pacific. Hence, we identify 1963/1964 as an El Niño Modoki event. As a matter of fact, we examined the evolution of SSTAs for every El Niño and El Niño Modoki event to choose these two events. In this study, we mainly use the composite method, and anomalies are calculated with respect to the base period of 1955–2005.

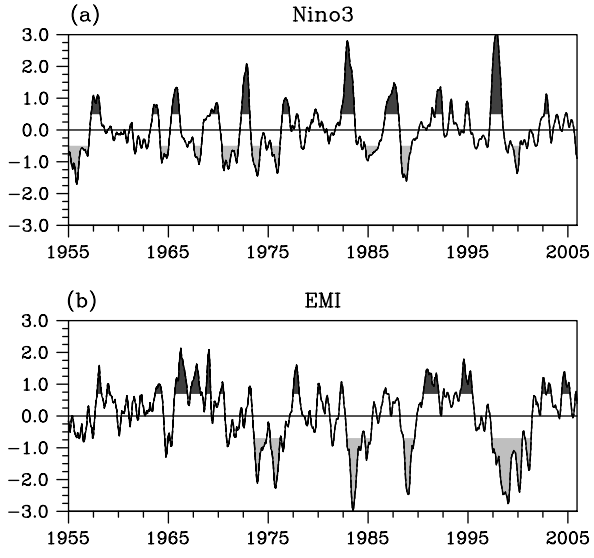

Figure 2. The time series of the normalized (a) Niño3 and (b) EMI for the period of 1955–2005. The black (or grey) shadings in (a) indicate Niño3 index greater than 0.5 (or less than −0.5). In (b) the black (or grey) shadings indicate EMI greater than 0.7 (or less than −0.7).

3. The rainfall anomalies related to El Niño and El Niño Modoki decaying phases

3.1. The evolution of SSTA

Figure 3 shows the evolution of composite SSTAs from the developing to the decaying phases of both El Niño and El Niño Modoki, and the shading indicates 95% confidence level which is calculated by a Student's *t*-test (Wilks, 1995). During canonical El Niño, a positive SSTA appears in the central and eastern Pacific while negative anomalies are seen over the western Pacific Rim during spring of the developing years. As El Niño evolves, the positive SSTA expands latitudinally and negative signals eastward, showing a prominent dipole pattern in the equatorial Pacific. The warm SSTA reaches it maximum amplitude in autumn and winter. Finally during summer of the decaying year, the warm SSTA disappears and is replaced by cool anomalies in the eastern Pacific.

In contrast, the evolution of El Niño Modoki is very different from that of El Niño. During El Niño Modoki, weak positive SSTAs first appear in the western Pacific during spring, and they subsequently move to the central Pacific in summer. At the same time, negative anomalies are found in the eastern and western Pacific. Together they display a tri-pole pattern rather than a dipole pattern associated with El Niño events. Note that the positive SSTA is still centred in the central Pacific, as it intensifies and extends eastward during autumn. In winter, the positive SSTA signals become strongest. This is followed by the decline of El Niño Modoki in the following spring and the tri-pole SSTA pattern disappears in the next season.

We can see that there are several obvious differences in the SSTA patterns between El Niño and El Niño Modoki. First, warm SSTAs are mainly confined to the eastern Pacific for El Niño events while they are maintained in the central Pacific during El Niño Modoki. Second, SSTAs decay more rapidly in El Niño Modoki than those in El Niño. Third, the magnitude of the SST signals in El Niño Modoki is weaker than that in El Niño, although the El Niño Modoki happened in a warmer background SST (Kim *et al*., 2009). These different SSTA patterns are expected to lead to different atmospheric responses.

3.2. Rainfall anomaly over China

Chinese rainfall experiences a striking annual variation with a wet season in boreal summer, a dry season in boreal winter and transition seasons in boreal spring

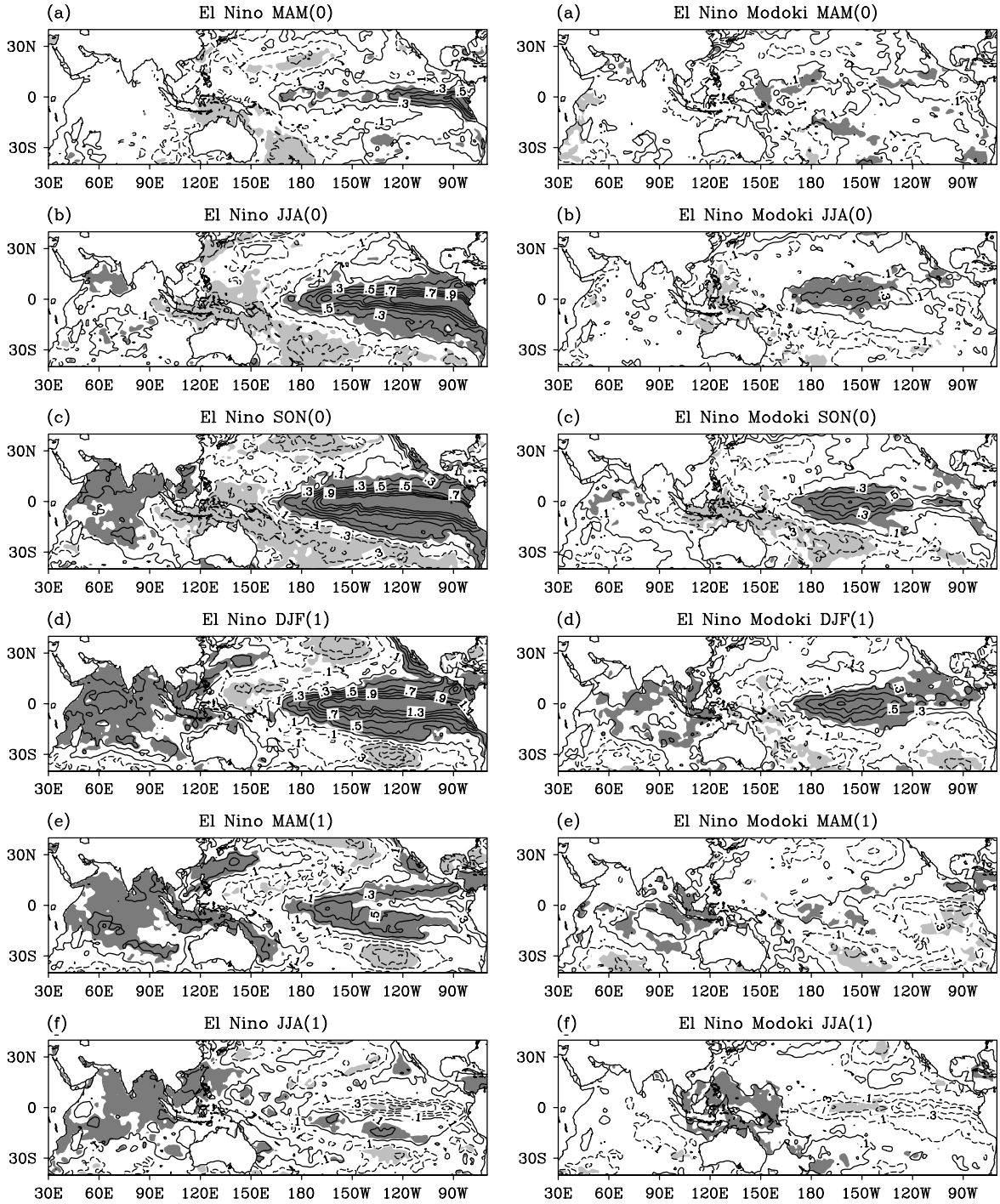

Figure 3. Evolution of composite SST anomalies from the developing year (0) to the decaying year (1) for El Niño and El Niño Modoki events with (a) MAM (0), (b) JJA (0), (c) SON (0), (d) DJF (1), (e) MAM (1) and (f) JJA (1). The left column is for the El Niño years and the right one is for the El Niño Modoki years. Contour interval is 0.2 °C and zero contour lines are omitted. The shading indicates 95% confidence level which is calculated by a Student's t test.

and autumn (Figure 4). Figure 5 shows the percentage and variance of rainfall in spring and summer. In South China, the fraction of springtime rainfall to the annual mean is about 35–40%, which is higher than that in summer (Figure 5(a) and (b)). At the same time, there is also significant inter-annual variability during spring for South China (Figure 5(c)). In other words, the spring precipitation variations play an important role for the total precipitation received over South China. For most other geographical locations, the summer rainfall generally occupies the largest part of total annual rainfall (Figure 5(b)). The variance is large in the whole of eastern China, especially in the Yangtze River Valley (Figure 5(d)). Hence, we focus on the spring and summer rainfall on the basis of the above consideration. Here, attention is mainly paid to the rainfall changes in spring and summer for the decaying phases of El Niño and El Niño Modoki.

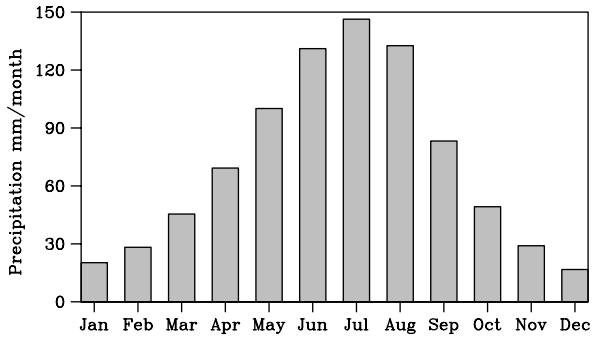

Figure 4. The annual variation of rainfall over China (mm/month) averaged from 1955 to 2005.

To uncover where the China rainfall anomalies experience the most noticeable differences, we compare the composite rainfall anomalies in the spring and summer of the decaying year for both El Niño and El Niño Modoki events by using the rainfall data in 160 stations of China. The composite results display remarkable differences between these two phenomena (Figure 6). In spring, significant rainfall anomalies appear in southern China for decaying El Niño events (Figure 6(a)). However, there are no significant rainfall variations in the same stage for El Niño Modoki (Figure 6(b)). In summer, negative rainfall anomalies appear in the Yangtze–Huaihe River Valley and positive anomalies are present in northern China as well as the south of the Yangtze River for El Niño events (Figure 6(c)). This is consistent with previous studies (e.g. Huang and Wu, 1989; Chen, 2002). In contrast, for El Niño Modoki, positive precipitation anomalies are mainly located in the Yellow–Huaihe River Valley and the precipitation tends to be below-normal to the south of the Yangtze River (Figure 6(d)). Apparently, the largest contrast of the rainfall anomalies between these two phenomena is found in the Yellow–Huaihe River Valley and in southern China.

4. Possible mechanisms responsible for the rainfall variations

4.1. Walker circulation

The Walker circulation is the significant tropical feature which involves the rising motion in the western Pacific and the Maritime Continent, upper-level westerly winds, the sinking motion in the eastern Pacific and easterly winds at the low level. The Walker circulation is sensitive to the SST variation, especially to the western Pacific 'warm pool' variability (Bjerknes, 1969). Figure 7 shows the anomalous velocity potential at 200 hPa which is adopted to reflect variations of the large-scale descending and ascending motions in the tropical region including those associated with the Walker circulation. During their mature phase, the velocity potential anomalies depict different patterns in the tropical Pacific, with a dipole for El Niño and a tri-pole for El Niño Modoki (Ashok *et al.*, 2007, 2009a); this is consistent with the different SSTA distributions associated with the two phenomena. For El Niño years, the anomalous Walker circulation features ascend over the eastern Pacific and descend over the western Pacific, whereas for El Niño Modoki it displays anomalous rising over the central Pacific and

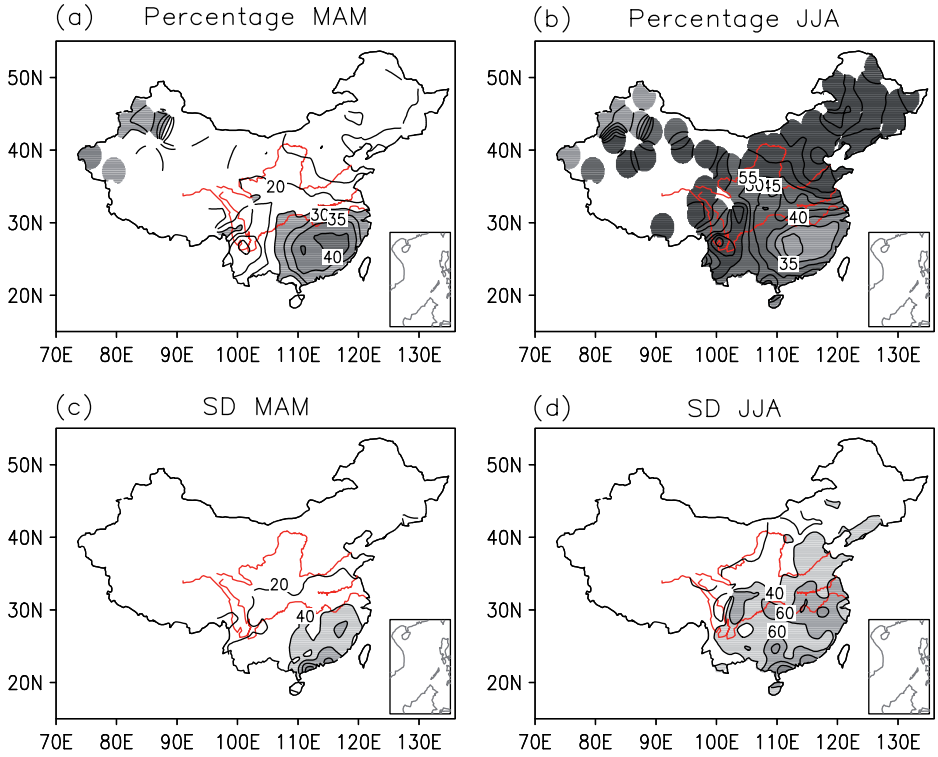

Figure 5. Percentage of annual total rainfall in (a) spring (MAM) and (b) summer (JJA). Standard deviation of the rainfall (mm/month) in (c) spring (MAM) and (d) summer (JJA). This figure is available in colour online at wileyonlinelibrary.com/journal/joc

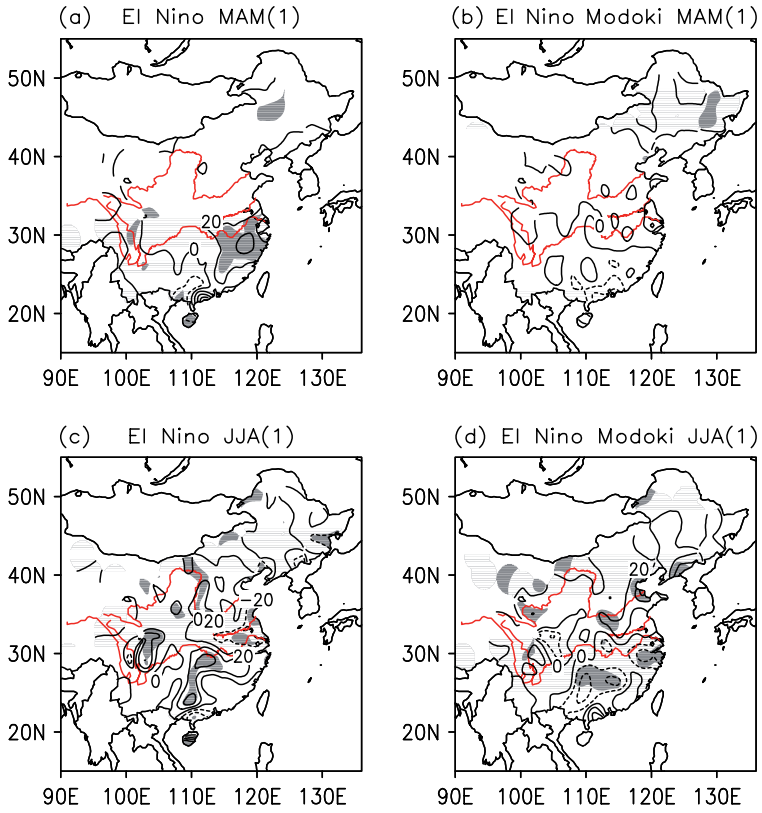

Figure 6. Composite rainfall anomalies during (a, b) MAM (1) and (c, d) JJA(1) in El Niño and El Niño Modoki decaying years. Contour interval is 20 mm/month. The shading indicates 95% confidence level. This figure is available in colour online at wileyonlinelibrary.com/journal/joc

sinking over the western and eastern Pacific (Figure 7(a)). The tri-pole pattern, however, evolves into a dipole in the spring of the decaying year for El Niño Modoki. From winter to the following summer, the locations of the divergent and convergent centres have an obvious change for both El Niño and El Niño Modoki events. However, the timing for the change is different. For El Niño, it happens in the following summer while for El Niño Modoki it occurs in the following spring. This difference may be induced by the different tropical SSTA distributions. In the following summer, the anomalous Walker circulation consists of ascent over the Indian Ocean possibly due to the capacitor effect (Xie *et al.*, 2009) and descent over the central Pacific in both El Niño and El Niño Modoki. But in the western Pacific, the anomalous divergent flow is more obvious in El Niño than that in El Niño Modoki, which demonstrates that the convection is more active during El Niño than that during El Niño Modoki. Thus, different convective conditions may lead to corresponding different East Asian atmospheric circulation anomalies.

4.2. Anomalous WNP anti-cyclone

Figure 8 shows the 850 hPa wind anomaly and the shading denotes the 90% confidence level. The evolutions of the anti-cyclone in the two phenomena are distinctively different. First, in the cases of El Niño, the WNP anti-cyclone develops in autumn and persists till the following summer, whereas for El Niño Modoki this anti-cyclone appears in winter and then becomes weak or even disappears in the following spring. Interestingly, the WNP circulation becomes anti-cyclonic again in summer. This distinction between El Niño and El Niño Modoki is possibly related to the different air–sea interaction involved (Kug *et al.*, 2009). Because of such a difference in the anomalous WNP anti-cyclone development, there are no obvious rainfall variations during El Niño Modoki in spring (Figure 6(b)), but heavy springtime precipitation over southern China was evoked by the anomalous anti-cyclone associated with El Niño (Figure 6(a)). Second, the anti-cyclonic flow in summer of the decaying El Niño Modoki events extends to higher latitudes around 40°N and the southwesterly winds over the western side of the anti-cyclone tend to carry abundant water vapour to the northern China, which induces above-normal rainfall over the Yellow–Huaihe River Valley. In contrast, this anti-cyclone in El Niño decaying summer can only stretch to about 25°N, which confines the water vapour transport to the south of the Yangtze River and leads to the deficient moisture over the Yangtze–Huaihe River Valley. The obvious anti-cyclone in the decaying summer for El Niño Modoki is consistent with the strong descent in the WNP (Figure 7(c)). Third, there is a striking difference in the atmospheric circulation associated with the two different types of El Niño during their decaying phase. During spring of the decaying year for El Niño Modoki, weak easterly winds are found over the central equatorial Pacific, which is opposite in direction to the westerly winds in the previous winter season; this might

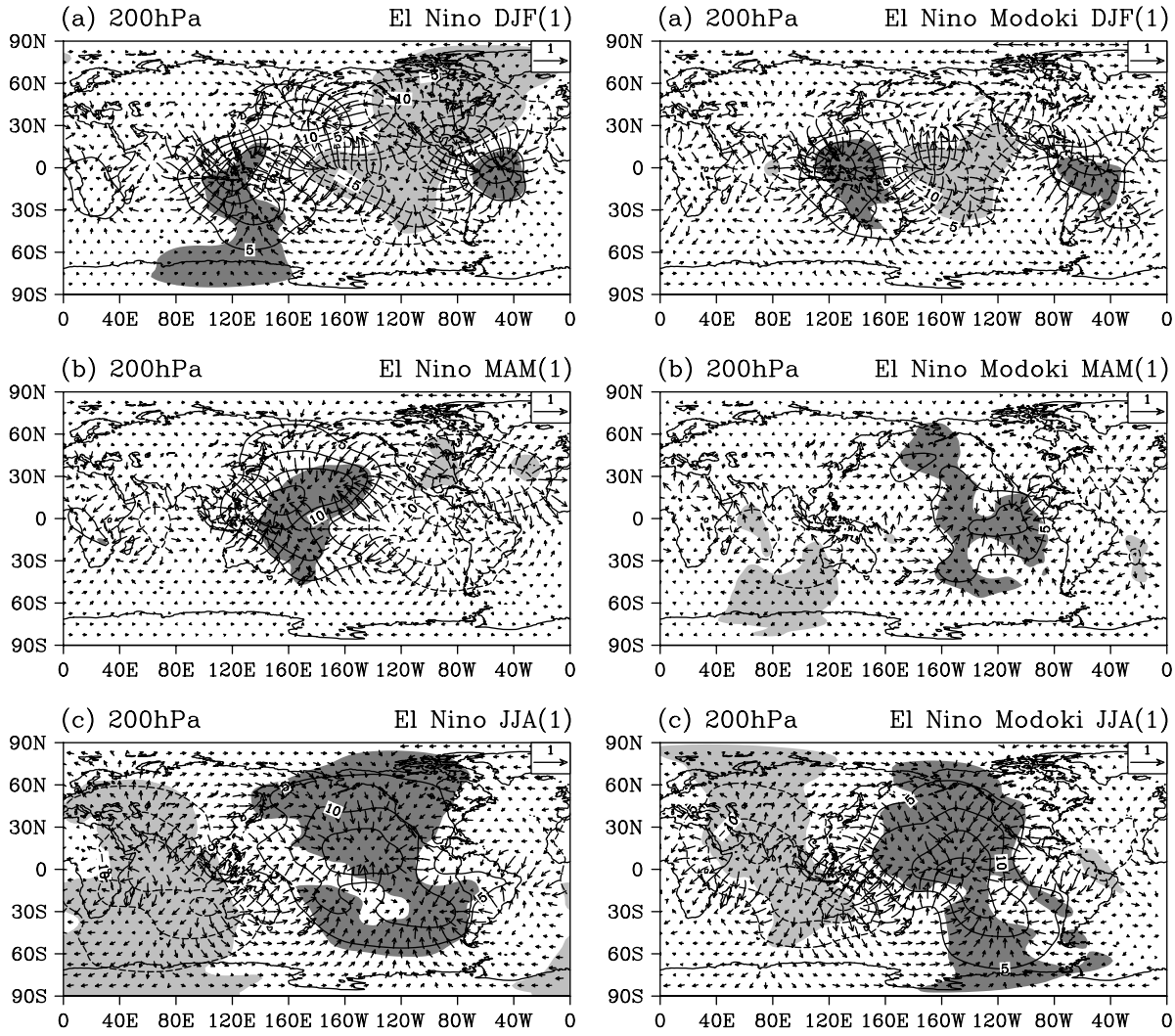

Figure 7. Composite 200 hPa velocity potential during (a) DJF (1), (b) MAM (1) and (c) JJA (1) in El Niño and El Niño Modoki events. The left column is for the El Niño events and the right one is for the El Niño Modoki events. Contour interval is 5×10^5 m^2/s. Zero contour lines are omitted. The shading indicates 95% confidence level.

help to accelerate the decay of El Niño Modoki. In contrast, anomalous easterly winds begin to appear over the central equatorial Pacific in summer for decaying El Niño events. That might explain why SSTA in El Niño reduces more slowly compared to that in El Niño Modoki events. Furthermore, the subsequent SSTA distributions for both El Niño and El Niño Modoki are examined. The negative SSTAs in the eastern Pacific are enhanced from the summer to the following winter. Hence, instead of a decaying El Niño Modoki event, the developing La Niña event probably facilitates the re-invigoration of the WNP anti-cyclonic flow in summer.

Recently, Xie *et al.* (2009) proposed a mechanism for the formation of the WNP anti-cyclone during the El Niño decaying summer. They suggest that El Niño-induced persisting warm SSTA in the tropical Indian Ocean may increase the tropospheric temperature, thereby exciting a Kelvin wave response in WNP. The WNP anti-cyclone can persist until summer by the Kelvin wave-induced Ekman divergence mechanism. In order to distinguish the different impacts of the tropical Indian Ocean SSTAs associated with the El Niño and El Niño Modoki on the anti-cyclone, we analyse the time-longitude section of the anomalous SST and zonal winds (Figure 9). For El Niño years, the SSTAs over the Indian Ocean become warm in the autumn of the developing phase and persist until the summer of the decaying phase. For El Niño Modoki events, the positive Indian Ocean SSTAs become very weak or even change into negative sign from May (1) to August (1) possibly due to the weak easterly wind anomalies over the Indian Ocean (Figure 9(b)). It is known that the onset of the southwesterly Indian monsoon is around the end of May. Therefore, anomalous easterly winds in the Indian Ocean act to weaken the Indian southwesterly winds over the Indian Ocean, which can give rise to the warm SSTA through the wind-evaporation SST feedback mechanism (Du *et al.*, 2009). Thus, the extremely weak easterly wind anomalies present there imply that there is no significant warm SSTA in the Indian Ocean during May (1) of the decaying El Niño Modoki. In June (1), the easterly winds intensify again but these winds only extend to 100 °E. This leads

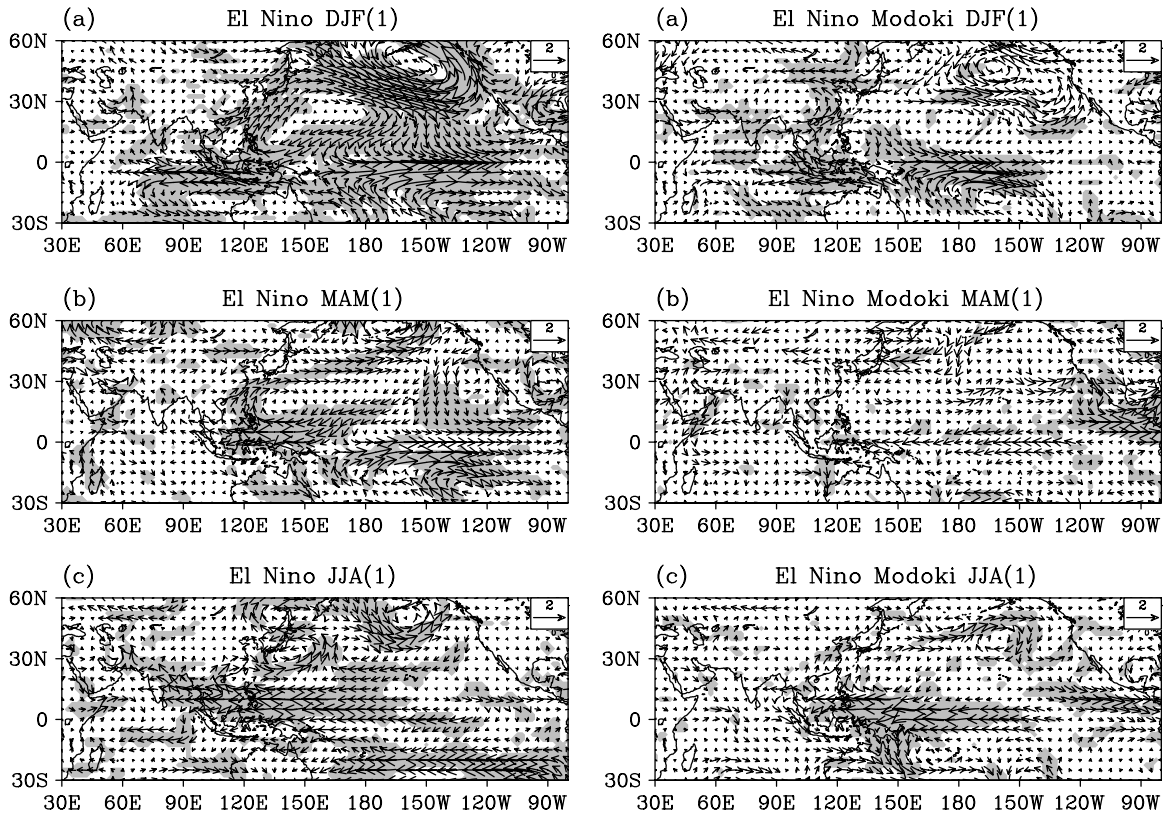

Figure 8. Composite 850 hPa wind anomalies (vectors; unit: m/s) during (a) DJF (1), (b) MAM (1) and (c)JJA (1) in El Niño and El Niño Modoki events. The left column is for the El Niño events and the right one is for the El Niño Modoki events. The shading indicates 90% confidence level.

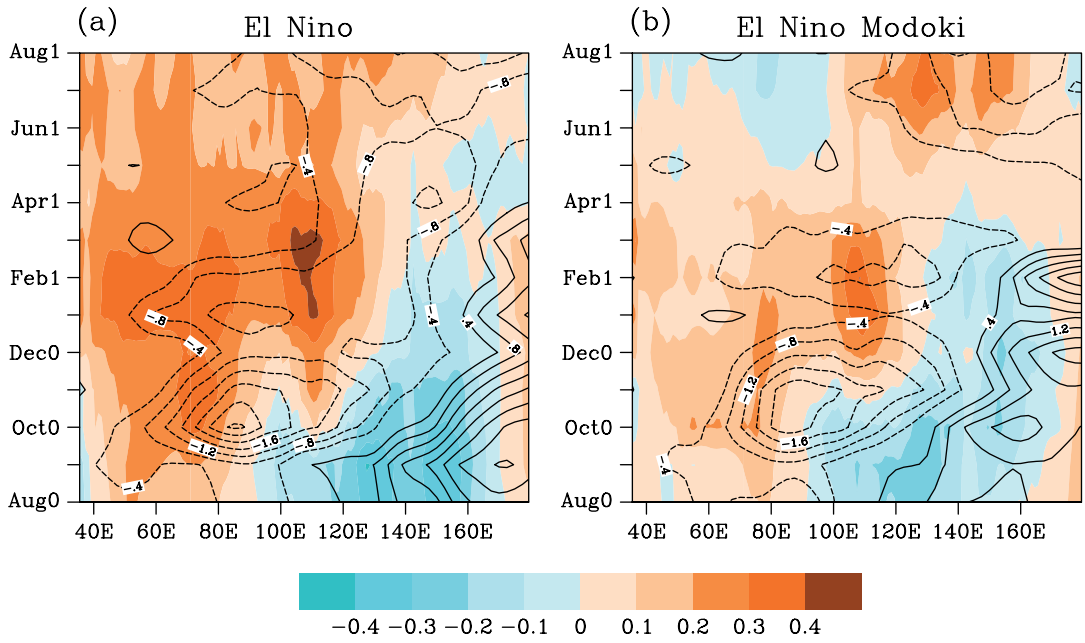

Figure 9. The time-longitude section of composite SST anomalies (shaded) averaged from 20 °S to 20°N and zonal winds (contour) averaged from 10 °S to 10°N for (a) El Niño and (b) El Niño Modoki events. This figure is available in colour online at wileyonlinelibrary.com/journal/joc

to warming of that part of the Indian Ocean and favours the positive SSTA in the east of 100 °E. Hence, the Indian Ocean capacitor effect on the WNP anti-cyclone in summer does not seem to take place in the decaying stage of El Niño Modoki.

China rainfall is influenced by the western Pacific sub-tropical high and the rainfall usually appears in the northwest of the sub-tropical high (Sun and Ying, 1999; Zhang *et al.*, 1999; Zhou *et al.*, 2005). The variability of the western Pacific sub-tropical high may be depicted by

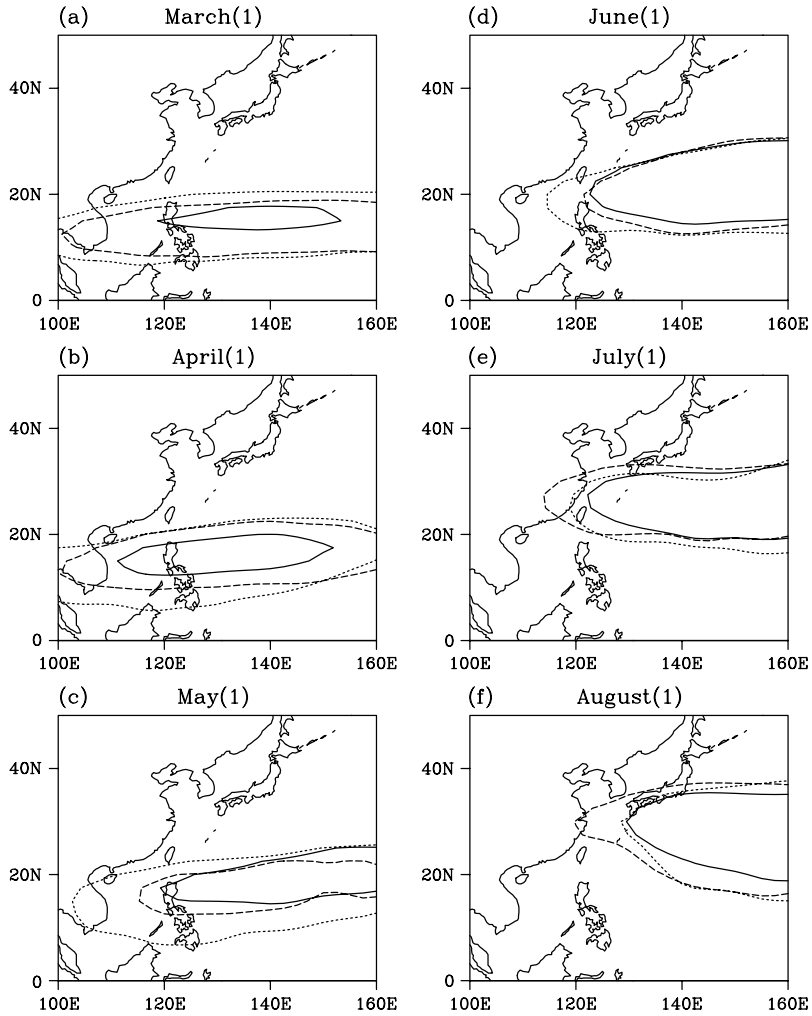

Figure 10. Composite western Pacific sub-tropical high with 5870 gpm contour in decaying El Niño and El Niño Modoki phases for (a) March, (b) April, (c) May, (d) June, (e) July and (f) August. The solid, short- and long-dashed lines indicate the climatological mean from 1955 to 2005, El Niño and El Niño Modoki events, respectively.

the WNP anti-cyclone as shown above. Here, we further show the monthly evolution of the sub-tropical high from spring to summer in the decaying phases of El Niño and El Niño Modoki. Figure 10 presents the composite WNP sub-tropical high which is defined by the area enclosed 5870 gpm contour of the 500 hPa geopotential height field in March (1), April (1), May (1), June (1), July (1) and August (1), respectively. During March (1) to April (1), the sub-tropical high extends substantially westward during both El Niño and El Niño Modoki years. The high retreats nearly to its climatological location during May (1) and June (1) in El Niño Modoki events. However, the high tends to be sustained till July (1) in El Niño cases. This is in favour of more rainfall in the south of the Yangtze River and less rainfall in the Huaihe River Valley, which is associated with the lower tropospheric WNP anomalous anti-cyclone. Interestingly, the sub-tropical high extends northwestward much into the inland region in July (1) and August (1) of the decaying El Niño Modoki. The location of the WNP anti-cyclone at the low level induces positive rainfall anomalies in the Yellow–Huaihe River Valley, where it is located in the northwestern edge of the sub-tropical high, and negative anomalies in the south of the Yangtze River, where it is now covered by the high-pressure system.

The water vapour transport is also important to the rainfall anomalies. We have computed the vertically integrated moisture fluxes and their divergence anomalies for both El Niño and El Niño Modoki events. Results are shown in Figure 11. The transportation of water vapour to eastern China is mainly caused by the WNP anti-cyclone. In the spring of the decaying year for El Niño, abundant water vapour is transported from the South China Sea by the southwesterly on the western side of the anti-cyclone, which favours above-normal rainfall south of the Yangtze River. Not surprisingly, there is no evident water vapour anomaly in spring during decaying El Niño Modoki, consistent with the normal WNP anti-cyclone condition (Figure 8(b)). During summer in the decaying year of El Niño, the moisture transportation consists of two parts: one from the western Pacific to South China and the other from the northern part of India to South China. Both are important for the heavy rainfall in the south of the Yangtze River. On the other hand, during the

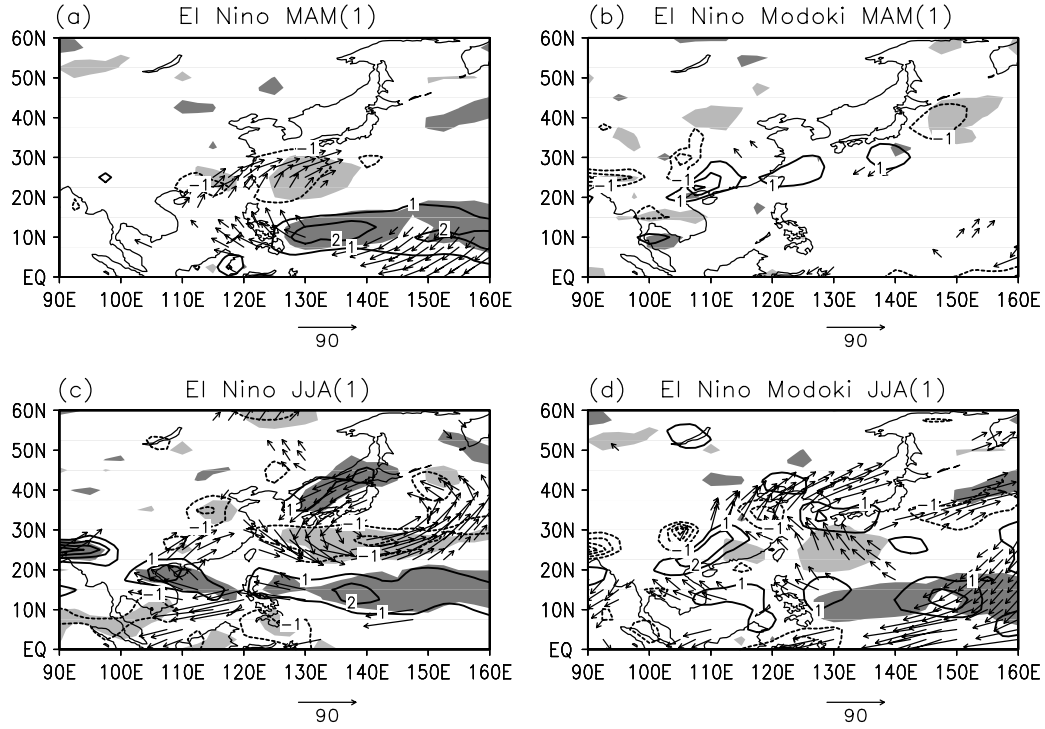

Figure 11. Composite vertically integrated water vapour flux (vector; unit: kg/m/s) and anomalous divergence (contours; unit: 10^{-5} kg/m^2/s) during (a, b) MAM (1) and (c, d) JJA (1) in El Niño and El Niño Modoki decaying years. The vectors less than 10 kg/m/s are omitted. The shading indicates 90% confidence level.

same season for decaying El Niño Modoki, anomalous southwesterly winds are seen to transport moisture to the Yellow–Huaihe River Valley where the moisture flux is convergent. Accordingly, there is above-normal rainfall over this region.

5. Discussions and conclusions

The impacts of El Niño and El Niño Modoki on China rainfall in their decaying phases are compared by using the re-analysis and the station rainfall data in the present study. Composite results indicate that these two events have remarkable different impacts on China rainfall. During spring in the decaying year of El Niño events, there are positive rainfall anomalies in the south of the Yangtze River. However, there are no significant rainfall anomalies in the same season for decaying El Niño Modoki. In the subsequent summer season, the wet signal south of the Yangtze River associated with El Niño continues, while suppressed rainfall appears in the Yangtze–Huaihe River Valley. In contrast, the rainfall is above normal in the region from the Huaihe River to the Yellow River, below normal in southern China during the summer of decaying El Niño Modoki events.

Possible physical process by which El Niño and El Niño Modoki affects the precipitation in China is investigated, too. Particularly, the anomalous WNP anti-cyclone associated with these two events is studied, which can induce the sub-tropical high variations and directly influence the water vapour transport. During spring in the decaying year of El Niño events, this anti-cyclone shifts the ridge of the sub-tropical high westward in both spring and summer; meanwhile, the anomalous southerly flow over the western edge of the anti-cyclone transports extra moisture from the South China Sea to southern China. At the same time, the eastward warm advection at 500 hPa from the eastern flank of Tibetan Plateau facilitates the convection by inducing adiabatic ascent (Sampe and Xie, 2010). These tend to cause above-normal rainfall in the southern Chinese region. In contrast, during spring in the decaying year of El Niño Modoki events, the anomalous WNP anti-cyclone becomes weak. As a result, there are no significant rainfall anomalies in China. In summer, however, the anomalous WNP anti-cyclone intensifies and extends more northwestward towards the inland region, compared to its El Niño counterpart. At the same time, the sub-tropical high associated with this anti-cyclone is intensified with a westward shift, especially in July and August. Hence, the southerly wind anomalies on the western side of the anti-cyclone extend to northern China and bring plentiful moisture to the region from the Huaihe River to the Yellow River. Hence, above-normal rainfall tends to appear in this region, while below-normal rainfall tends to occur in the southern part of the Yangtze River Valley where it is covered by the sub-tropical high.

For both El Niño and El Niño Modoki events, the anomalous WNP anti-cyclone is meaningful for China rainfall variations so that we checked the Indian Ocean capacitor effect on this anti-cyclone as proposed by Xie *et al.* (2009). In El Niño decaying years, the anomalous easterly winds over the equator weaken the southwesterly monsoon over India and induce warming SSTAs in the

Indian Ocean (Yuan *et al*., 2008a, 2008b). Thus, the summer WNP anti-cyclone may be maintained by the Kelvin wave-Ekman divergence mechanism. In contrast, in El Niño Modoki decaying years, the evolution of the SSTAs in the Indian Ocean is different from that in El Niño events. The warm SSTAs tend to be weak in the spring of the decaying years and even become cold SSTAs in summer. Hence, the Indian Ocean capacitor effect on the summer WNP anti-cyclone seems not to occur in the decaying phase of El Niño Modoki. However, the developing La Niña event after the fast dissipation of El Niño Modoki may anchor the summer climate anomalies.

Acknowledgements

This work is supported jointly by the National Key Technology R&D Program of China (Grant 2008BAK50B02), the National Basic Research Program of China (Grants 2009CB421401 and 2009CB421405) and the Joint National Natural Science Foundation of China (Grant U0733002).

References

Ashok K, Behera S, Rao S, Weng H, Yamagata T. 2007. El Niño Modoki and its possible teleconnection. *Journal of Geophysical Research* **112**: C11007, DOI: 10.1029/2006/JC003798.

Ashok K, Iizuka S, Rao S, Saji N, Lee W. 2009a. Processes and boreal summer impacts of the 2004 El Niño Modoki: an AGCM study. *Geophysical Research Letters* **36**: L04703, DOI: 10.1029/2008GL036313.

Ashok K, Tam CY, Lee WJ. 2009b. ENSO Modoki impact on the Southern Hemisphere storm track activity during extended austral winter. *Geophysical Research Letters* **36**: L12705, DOI:10.1029/2009GL038847.

Bao M, Han R. 2009. Delayed impacts of the El Niño episodes in the central Pacific on the summertime climate anomalies of eastern China in 2003 and 2007. *Advances in Atmospheric Sciences* **26**: 553–563.

Bjerknes J. 1969. Atmospheric teleconnections from the equatorial Pacific. *Monthly Weather Review* **97**: 163–172.

Chan JCL, Zhou W. 2005. PDO, ENSO and the early summer monsoon rainfall over South China. *Geophysical Research Letters* **32**: L08810, DOI: 10.1029/2004GL022015.

Chang C, Zhang Y, Li T. 2000. Interannual and interdecadal variations of the East Asian summer monsoon and tropical Pacific SSTs. Part I: roles of the subtropical ridge. *Journal of Climate* **13**: 4310–4325.

Chen W. 2002. Impacts of El Niño and La Niña on the cycle of the East Asian winter and summer monsoon. *Chinese Journal of Atmospheric Sciences* **26**: 595–610 (in Chinese).

Du Y, Xie SP, Huang G, Hu K. 2009. Role of air-sea interaction in the long persistence of El Niño-induced North Indian Ocean warming. *Journal of Climate* **22**: 2023–2038.

Duchon C. 1979. Lanczos filtering in one and two dimensions. *Journal of Applied Meteorology* **18**: 1061–1022.

Huang R, Chen W, Yan B, Zhang R. 2004. Recent advances in studies of the interaction between the East Asian winter and summer monsoon and ENSO cycle. *Advances in Atmospheric Sciences* **21**: 407–424.

Huang P, Huang R. 2009. Relationship between the modes of winter tropical sea surface temperature anomalies in the Pacific and the intraseasonal variations of the following summer rainfall anomalies in China. *Atmospheric and Oceanic Science Letters* **2**: 295–300.

Huang R, Wu Y. 1989. The influence of ENSO on the summer climate change in China and its mechanism. *Advances in Atmospheric Sciences* **6**: 21–32.

Kalnay E, Kanamitsu M, Kistler R, Collins W, Deaven D, Gandin L, Iredell M, Saha S, White G, Woollen J. 1996. The NCEP/NCAR 40-year reanalysis project. *Bulletin of the American Meteorological Society* **77**: 437–471.

Kim H, Webster P, Curry J. 2009. Impact of shifting patterns of Pacific Ocean warming on North Atlantic tropical cyclones. *Science* **325**: 77.

Kug J, Jin F, An S. 2009. Two types of El Niño events: cold tongue El Niño and warm pool El Niño. *Journal of Climate* **22**: 1499–1515.

Lin X, Yu S. 1993. El Niño and rainfall during the flood season (June-August) in China. *Acta Meteorologica Sinica* **51**: 434–441.

Liu Y, Ding Y. 1992. Influence of El Niño on weather and climate in China. *Acta Meteorologica Sinica* **6**: 117–131.

McPhaden M. 1999. Genesis and evolution of the 1997–1998 El Niño. *Science* **283**: 950–954.

McPhaden M. 2004. Evolution of the 2002/03 El Niño. *Bulletin of the American Meteorological Society* **85**: 677–695.

Picaut J, Hackert E, Busalacchi A, Murtugudde R, Lagerloef G. 2002. Mechanisms of the 1997–1998 El Niño–La Niña, as inferred from space-based observations. *Journal of Geophysical Research* **107**: 3037, DOI: 10.1029/2001JC000850.

Rayner N, Parker D, Horton E, Folland C, Alexander L, Rowell D, Kent E, Kaplan A. 2003. Global analyses of sea surface temperature, sea ice, and night marine air temperature since the late nineteenth century. *Journal of Geophysical Research* **108**: 4407, DOI: 10.1029/2002JD002670.

Sampe T, Xie SP. 2010. Large-scale dynamics of the Meiyu-Baiu rain band: Environmental forcing by the westerly jet. *Journal of Climate* **23**: 113–134.

Sun S, Ying M. 1999. Subtropical high anomalies over the western Pacific and its relations to the Asian monsoon and SST anomaly. *Advances in Atmospheric Sciences* **16**: 559–568.

Taschetto A, Ummenhofer C, Gupta A, England M. 2009. Effect of anomalous warming in the central Pacific on the Australian monsoon. *Geophysical Research Letters* **36**: L12704, DOI: 10.1029/2009GL038416.

Wang B, Wu R, Fu X. 2000. Pacific–East Asian teleconnection: how does ENSO affect East Asian climate? *Journal of Climate* **13**: 1517–1536.

Weng H, Ashok K, Behera S, Rao S, Yamagata T. 2007. Impacts of recent El Niño Modoki on dry/wet conditions in the Pacific rim during boreal summer. *Climate Dynamics* **29**: 113–129.

Weng H, Lau K, Xue Y. 1999. Multi-Scale summer rainfall variability over China and its long-term link to global sea surface temperature variability. *Journal of the Meteorological Society of Japan* **77**: 845–857.

Wilks D. 1995. *Statistical Methods in the Atmospheric Science: An introduction*. Academic: San Diego, CA, 139.

Wu R, Hu Z, Kirtman B. 2003. Evolution of ENSO-related rainfall anomalies in East Asia. *Journal of Climate* **16**: 3742–3758.

Xie SP, Du Y, Huang G, Zheng X, Tokinaga H, Hu K, Liu Q. 2010. Decadal shift in El Niño influences on Indo-western Pacific and East Asian climate in the 1970s. *Journal of Climate* **23**: 3352–3368.

Xie SP, Hu K, Hafner J, Tokinaga H, Du Y, Huang G, Sampe T. 2009. Indian Ocean capacitor effect on Indo–western Pacific Climate during the summer following El Niño. *Journal of Climate* **22**: 730–747.

Xue F, Liu C. 2008. The influence of moderate ENSO on summer rainfall in eastern China and its comparison with strong ENSO. *Chinese Science Bulletin* **53**: 791–800.

Yuan Y, Zhou W, Chan JCL, Li C. 2008a. Impacts of the basin-wide Indian Ocean SSTA on the South China Sea summer monsoon onset. *International Journal of Climatology* **28**: 1579–1587, DOI:10.1002/JOC.1671.

Yuan Y, Zhou W, Yang H, Li C. 2008b. Warming in the northwestern Indian Ocean associated with the El NiNo event. *Advances in Atmospheric Sciences* **25**: 246–252.

Zhang R, Sumi A. 1999. A diagnostic study of the impact of El Niño on the precipitation in China. *Advances in Atmospheric Sciences* **16**: 229–241.

Zhang R, Sumi A, Kimoto M. 1996. Impact of El Niño on the East Asian monsoon: a diagnostic study of the'86/87 and'91/92 events. *Journal of the Meteorological Society of Japan* **74**: 49–62.

Zhou W, Chan JCL. 2007. ENSO and the South China Sea summer monsoon onset. *International Journal of Climatology* **27**: 157–167.

Zhou W, Chan JCL, Li C. 2005. South China Sea summer monsoon onset in relation to the off-equatorial ITCZ. *Advances in Atmospheric Sciences* **22**: 665–676.

Zhou LT, Tam CY, Zhou W, Chan JCL. 2009. Influence of South China Sea SST and the ENSO on winter rainfall over South China. *Advances in Atmospheric Sciences* **27**: 832–844, DOI: 10.1007/s00376-009-9102-7.

